

Thermoacoustic Refrigeration: Short Review

Omar Ahmed Al-Mufti ^a and Isam Janajreh ^{a*}

^a Department of Mechanical Engineering, Khalifa University of Science and Technology, Abu Dhabi, UAE

Abstract

Thermoacoustic is the science that studies the conversion of the heat into acoustical sound and vice versa. The conversion of heat to acoustic power is done through Thermoacoustic engine (TAE). This generated acoustic power can be converted to another and useful form such as mechanical or electrical energy. On the other hand, Thermoacoustic refrigerator (TAR) or heat pump is a device that uses acoustic sound to pump heat from a lower temperature reservoir. The most distinct feature of thermoacoustic systems is that they do not have moving parts, which makes them reliable. Thermoacoustic engine can recycle any source of waste heat and use sustainable heat like concentrated solar. Also, in contrast to conventional refrigeration methods, thermoacoustic refrigerator spares the usage of environmentally harmful gases that is daunting the centralized cooling industry. There is no doubt the thermoacoustic technology has been considered in various applications with some unspoken advancement. In this manuscript we intend to review the fundamentals of thermoacoustics and highlight their recent developments. Additionally, analytical simulation of thermoacoustic refrigerator will be discussed and validated against experimental published work. The goal is to reveal the effect of different parameters on the performance in an attempt to establish design guidelines for an improved technology metrics. The future prospects of thermoacoustic refrigeration are also presented at the end of this study.

Keywords: *Thermoacoustic engine; Thermoacoustic refrigerator; Thermal and viscous penetration depth; Standing and traveling wave*

1. Introduction

Thermoacoustic is a science that involves both thermodynamics and acoustics. It studies the conversion of heat into acoustic waves or vice versa. Thermoacoustic engine (TAE) or prime mover is the device that harnesses heat to produce acoustic waves, which can be converted to useful mechanical or downstream electrical energy. Thermoacoustic refrigerator (TAR) or heat pump is the device that uses acoustic energy to pump heat from a lower temperature reservoir. Figs. 1(a) and 1(b) show the schematics for TAE and TAR, respectively. Generally, the main components of thermoacoustic systems are a resonant tube filled with a working gas such as air, He, Ar, CO₂, or their mixtures, cold and hot heat exchangers, a stack, and a source of acoustic power if TAR is utilized. Acoustic waves can be described as coupled longitudinal displacement and pressure oscillations [1]. The variation in pressure causes the temperature to oscillate too. Thermoacoustic devices can be

classified based on the type of wave, i.e., standing wave and traveling wave systems. Mainly, the design of the system and the operating conditions determine whether the acoustic wave in the system is traveling or standing. In traveling wave systems, the stack is called regenerator. The difference between the regenerator and the stack is that the stack has poor thermal contact with the working fluid, while the regenerator has perfect thermal contact. Thus, traveling wave can attain higher efficiencies.

* Corresponding author. Tel.: +971 2 312 3286

Fax: +971 2 312 3286; E-mail: isam.janajreh@ku.ac.ae

© 2016 International Association for Sharing Knowledge and Sustainability

DOI: 10.5383/ijtee.19.01.005

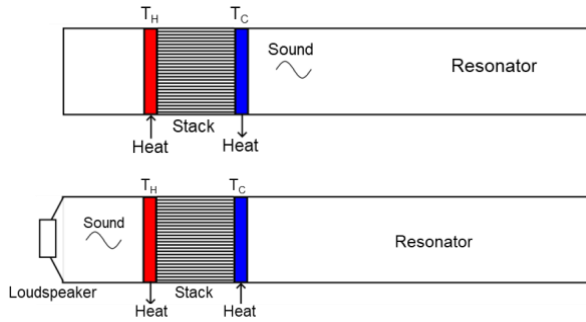


Fig. 1. (a) Thermoacoustic engine, (b) Thermoacoustic refrigerator

One of the first discoveries of using heat to generate sound was the Sondhauss tube in 1850 [2]. As shown in Fig. 2, it is open at one end and closed at the other end by a bulb. It was noticed that heating the gas which is close to the closed end steadily generates sound. Rayleigh was the first to give a description of this phenomenon [3]. He discovered that the sound generation occurs due to oscillatory thermal compression and expansion. A general explanation by Raleigh was that the vibration of air is stimulated by giving heat to the air at the peak of compression or drawing heat from at the peak of rarefaction. This gives a qualitative description of how thermoacoustic systems work. However, an accurate theory of thermoacoustic was not developed until 1969 by Nikolaus Rott [4] who then summarized his results in 1980 review [5]. The review is considered as a cornerstone of thermoacoustic field. One of the first practical thermoacoustic engines was built in Los Alamos National Laboratory (LANL) [6]. The first thermoacoustic refrigerator was also built in LANL, and it used a loudspeaker as an acoustic driver [7, 8]. Additionally, Backhaus and Swift [9] managed to design a traveling wave engine that combines the toroidal geometry with a resonator tube. Based on Rott’s work, in 1988, Swift [10] published a review paper that gives a comprehensive analysis of the thermodynamics of thermoacoustic systems. One of the commercial applications is the “green” freezer, which was built and used by Ben and Jerry ice cream brand [11, 12]. Another one is Sound Energy Ltd solar-driven roof top thermoacoustic cooler for air conditioning. The first product is already installed in Netherlands earlier this year (2022) [13].

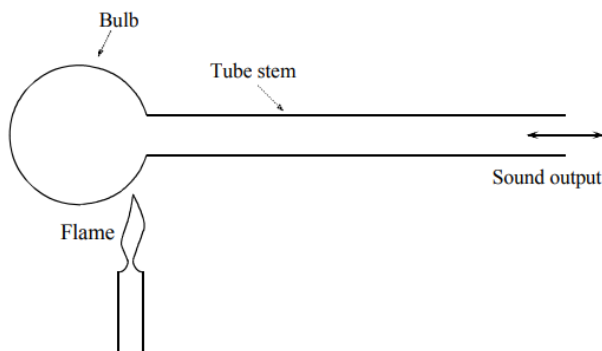


Fig. 2. Sondhauss tube [14]

In terms of refrigeration, the motivation comes from the fact that the demand for refrigeration is on the rise particularly that avoid the use of chemicals (i.e., HFCs and CFCs) which are not environment-friendly [15]. Also, sustainable cooling methods should be explored. Thermoacoustic refrigeration is one of the potential methods for sustainable cooling. First, thermoacoustic systems have almost no moving parts, which make them very reliable [1]. Second, they are usually easy and inexpensive to manufacture. Third, they could harness solar or waste heat to

generate acoustic waves that are used to run a thermoacoustic refrigerator [16]. All of these make TAR very promising to replace the current conventional cooling systems in many applications, including: air conditioning for buildings and vehicles [17, 18], natural gas liquefaction [19, 20], thermoacoustically driven thermoacoustic refrigerator [16, 17], and electronics cooling [21-24], which is done through miniaturized compact designs.

2. Thermoacoustic Basics

The fundamentals of thermoacoustic are presented here which include wave types, thermodynamic cycle, thermodynamic performance, and the short stack approximation.

2.1. Wave Types

There are two types of waves that are generated inside the thermoacoustic device, these are the standing and the traveling wave. The standing wave can be described as fluid parcels oscillating in a closed tube. Fig. 3(a) shows the pressure and velocity oscillations in a half wavelength tube. The arrows in the figure depicts the parcels oscillations with time. It should be noted that the velocity at the two ends of the tube remains constant, while the pressure oscillation is at its maximum. This point is called velocity node or pressure anti-node. On the other hand, the pressure stays constant in the middle of the tube, while the velocity variation is at a maximum. Thus, a pressure node/velocity anti-node is located at the middle of the tube. Fig. 3(b) illustrates the temperature and displacement oscillations in the tube. It can be clearly noticed that the temperature oscillation is maximum at the ends of tube, and minimum at the middle, which is identical to pressure oscillation. The displacement varies the most in the middle of the tube where the velocity oscillates the most. This figure indicates that the stack in standing wave systems should be placed somewhere between the pressure node and anti-node, where both temperature and displacement oscillations occur.

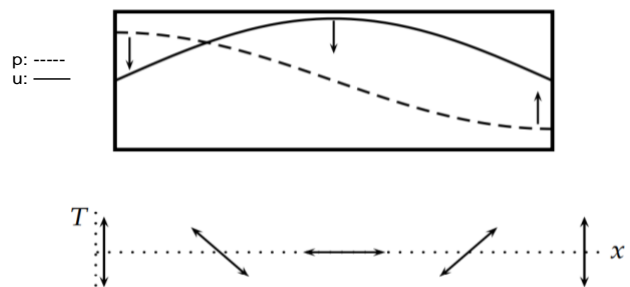


Fig. 3. (a) Standing wave pressure and velocity oscillations, (b) Standing wave temperature oscillations and displacement [25]

The traveling wave can be described as fluid parcels oscillating in an infinite tube. Thereby, neither pressure nor velocity nodes do exist. Fig. 4(a) illustrates the pressure and velocity oscillations in the tube. It can be noticed that all fluid parcels in the tube undergo the same pressure and velocity oscillations. Contrary to standing wave, the pressure and velocity are in phase and reach their maximum value at the same time and position as illustrated in Fig. 4. The temperature changes the most when the displacement is minimal, and the highest displacement occurs when the temperature is almost constant. This results in a circular temperature-position cycles as shown in Fig. 4(b). The absence of velocity and pressure nodes is the reason of having identical temperature-position cycles anywhere in the tube.

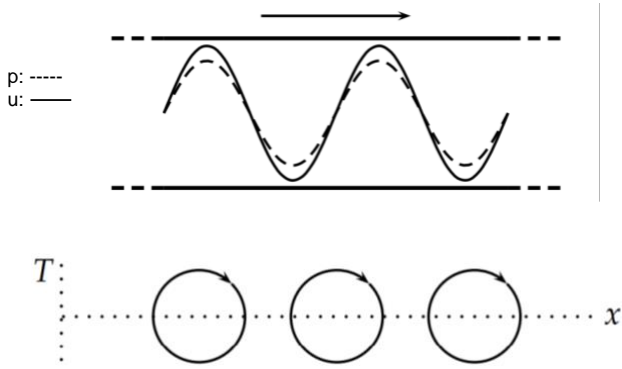


Fig. 4. (a) Traveling wave pressure and velocity oscillations, b) Traveling wave temperature oscillations and displacement [25]

2.2. Thermodynamic Cycles

From thermodynamic perspective, standing and traveling wave devices operates differently. For the standing wave, gas parcels undergo pressure and velocity oscillations with 90° out of phase angle. Fig. 5 illustrate such oscillations and it shows the compression happens at the peak pressure, while the displacement occurs at the peak velocity. The position of the parcel as a function of time can be easily found by integrating the velocity with respect to time. It ensures the parcel displacement and pressure are synchronized. This means that highest change in position occurs simultaneously under compression. Similarly, the expansion is also synchronized with the displacement, but in the opposite direction.

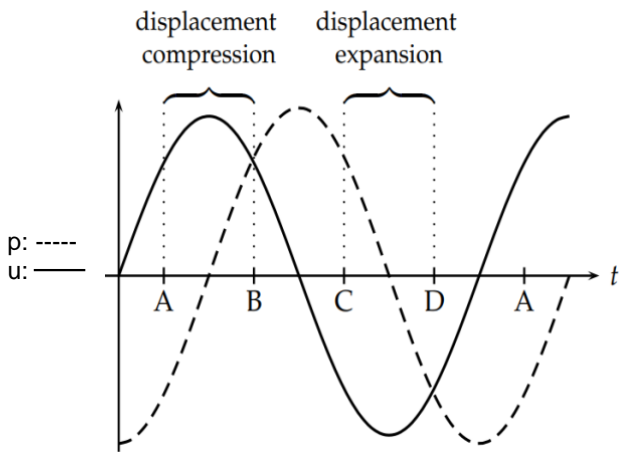


Fig. 5. Standing wave pressure and velocity oscillations with time [25]

Considering a gas parcel oscillating at a distance y over the plate having a temperature gradient $\Delta T/\Delta x$, three scenarios are possible. Firstly, if the gas parcel is far away from the plate ($y \gg \delta_k$ where δ_k is the thermal penetration length), there will be no heat exchange between the plate and gas parcel. Hence, the gas parcel will undergo compression and expansion adiabatically as there is no temperature gradient. Secondly, when the distance between the gas parcel and the plate is extremely small ($y \ll \delta_k$ the thermal contact is perfect) then the heating/cooling process will happen simultaneously, i.e., with both compression and displacement processes. The gas parcel in this case will have the same exact temperature profile as the plate. Therefore, it will not absorb/reject heat as it oscillates over

the stack, meaning no acoustic power is consumed nor produced. Thirdly, considering the distance between the gas parcel and the plate is almost equal to the thermal penetration depth ($y \sim \delta_k$), the thermal contact is imperfect or poor. Thus, the heating/cooling process will be delayed from the compression/expansion and displacement process. In other words, the gas parcel will be compressed and displaced towards the hot end, to be heated (TAE) or cooled (TAR) at the end of the stack. Afterwards, it gets expanded and displaced simultaneously, and finally is cooled (TAE) or heated (TAR) at the other end. The standing wave system operates as TAE when the temperature gradient of the plate is higher than the critical temperature gradient, while it operates as TAR if the temperature gradient is lower than the critical temperature gradient. Therefore, the operation of standing wave systems can be described as four-steps cycle as shown in Fig. 6, and summarized below:

- A-B: Isentropic compression
- B-C: Isobaric heat addition for TAE / heat rejection for TAR
- C-D: Isentropic expansion
- D-A: Isobaric heat rejection for TAE / heat addition for TAR

This cycle is identical to the Brayton cycle, however, the actual cycle follows an ellipsoid shape. Fig. 6 shows the ideal and real cycles for standing wave TAE and TAR and are also presented schematically along the stack locations.

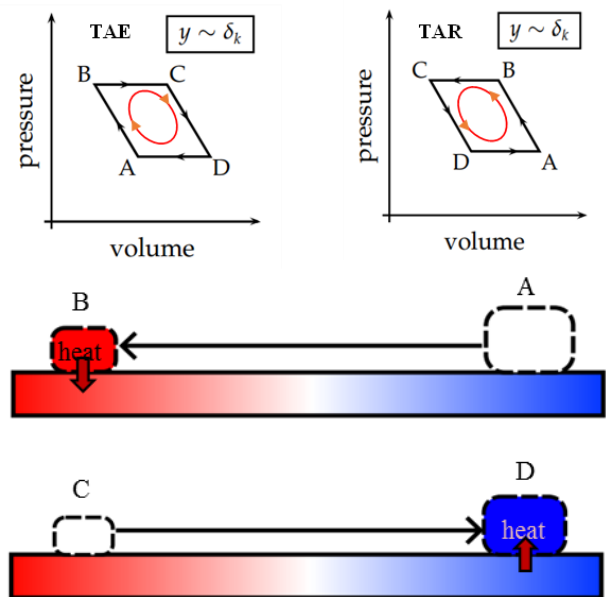


Fig. 6. Operating cycle for standing wave TAE and TAR [25]

As for the traveling wave, gas parcels undergo in-phase pressure and velocity oscillations, and the cycle is illustrated in Fig. 7 for the TAE and TAR. The in-phase oscillations cause the compression/expansion and displacement to occur sequentially. This means that a time delay of the heating/cooling process is not needed to create a four-step cycle. A perfect thermal contact ($y \ll \delta_k$) is required to maintain a heating/cooling simultaneously with the displacement. Thus, the four-step cycle is as follows:

- A-B: Isothermal compression
- B-C: Isochoric heat addition for TAE / heat rejection for TAR
- C-D: Isothermal expansion
- D-A: Isochoric heat rejection for TAE / heat expansion for TAR

This is identical to Stirling cycle, but the actual cycle has an ellipsoid shape. Fig. 8 shows both the ideal and actual traveling wave cycles for TAE and TAR and the schematic for four-step processes along the stack locations for TAE.

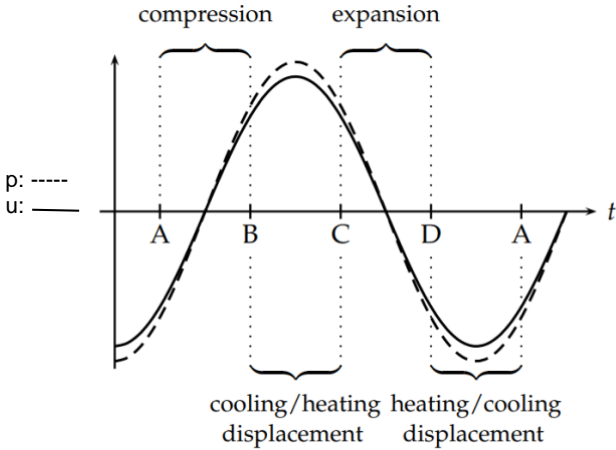


Fig. 7. Traveling wave pressure and velocity oscillations with time [25]

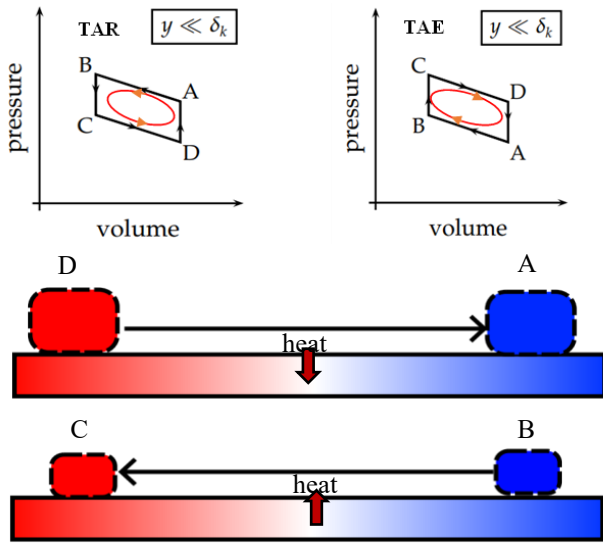


Fig. 8. Operating cycle for traveling wave TAR and TAE [25]

2.3. Parameters Of The Thermoacoustic Devices

The critical temperature gradient (ΔT_{crit}), which is mentioned earlier, is the boundary between the prime mover and the refrigerator. It can be calculated for the standing wave systems using Eq. 1 [10] as:

$$\Delta T_{crit} = \frac{T_m \beta \omega |p_1^s|}{\rho_m c_p |u_1^s|} \quad (1)$$

where T is temperature, β is the thermal expansion coefficient, ρ is density, ω is the angular frequency, c_p is fluid's specific heat, and p_1 and u_1 are the complex oscillating pressure and

velocity, respectively. The subscript "m" refers to the mean value, while the superscript "s" refers to standing wave. The thermal penetration depth (δ_k) is defined as the distance that the heat can diffuse through the fluid during a time of $1/\omega$ and is expressed in Eq. 2 as:

$$\delta_k = \sqrt{2K_g / \omega \rho_m c_p} \quad (2)$$

where K_g is the thermal conductivity of the fluid. The viscous penetration depth (δ_v) is similar to the thermal penetration depth but for viscosity effects, it is expressed in Eq. 3 as:

$$\delta_v = \sqrt{2\mu / \omega \rho_m} \quad (3)$$

where μ is the dynamic viscosity. Additionally, other important parameters used in thermoacoustic system are all summarized in Table 1 with their definitions.

Table 1: List of common thermoacoustic parameters

Parameter	Expression
Displacement amplitude	$ \xi_1 = \frac{ u_1 }{\omega}$ (4)
Wavelength	$\lambda = \frac{a}{f}$ (5) where a is the speed of sound in the fluid and f is the frequency
Wave number	$k = \frac{2\pi}{\lambda} = \frac{\omega}{a}$ (6)
Angular frequency	$\omega = 2\pi f$ (7)
Drive ratio	$D = \frac{p_0}{p_m}$ (8) where p_0 is pressure amplitude, and p_m is the mean pressure
Blockage ratio (porosity)	$B = \frac{y}{y+l}$ (9) where y is the spacing between plates, and l is the thickness of the plate
Prandtl number	$\sigma = \left(\frac{\delta_k}{\delta_k}\right)^2 = \frac{\mu c_p}{K_g}$ (10)
Mach number	$M = \frac{p_0}{p_m a^2}$ (11)

Typically, the displacement of one fluid parcel is small compared to the length of the stack/regenerator. Therefore, as shown in Fig. 9, there will be an entire train of adjacent fluid parcels, each confined to a short region passing on heat as in a bucket brigade.

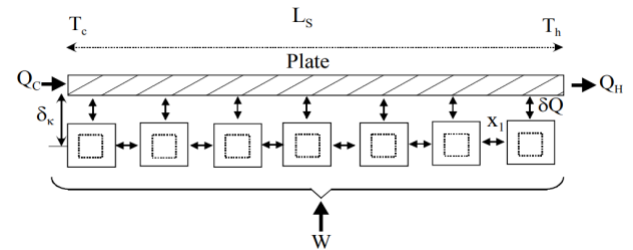


Fig. 9. Bucket-brigade effect in thermoacoustic refrigerator [14]

The performance of the TAE and TAR is thermodynamically assess by the two common metrics, the efficiency (η) and the

coefficient of performance (COP). These are also summarized in Table 2.

Table 2: Standard performance metrics for thermoacoustic devices

Metric	Expression
TAE Efficiency	$\eta = \frac{\dot{W}}{\dot{Q}_H} = \frac{\dot{Q}_H - \dot{Q}_C}{\dot{Q}_H} \quad (12)$ <p>where \dot{W} is the acoustic power, \dot{Q}_H is the heat added to the hot heat exchanger, and \dot{Q}_C is the heat rejected from the cold heat exchanger</p>
TAE Carnot Efficiency	$\eta_C = 1 - \frac{T_C}{T_H} \quad (13)$ <p>where T_C is the temperature at cold heat exchanger, and T_H is temperature at hot heat exchanger</p>
TAE Relative Efficiency	$\eta_R = \frac{\eta}{\eta_C} \quad (14)$
TAR Coefficient of performance	$COP = \frac{\dot{Q}_C}{\dot{W}} = \frac{\dot{Q}_C}{\dot{Q}_H - \dot{Q}_C} \quad (15)$ <p>where \dot{W} is the acoustic power, \dot{Q}_H is the heat removed from the hot heat exchanger, and \dot{Q}_C is the heat added to the cold heat exchanger,</p>
TAR Carnot coefficient of performance	$COP_C = \frac{T_C}{T_H - T_C} \quad (16)$ <p>where T_C is the temperature at cold heat exchanger, and T_H is temperature at hot heat exchanger</p>
TAR Relative coefficient of performance	$COP_R = \frac{COP}{COP_C} \quad (17)$

Based on the Rott's linear theory, where the momentum, continuity, and heat transfer equations were linearized, Swift [10] derived the generated/absorbed acoustic power (\dot{W}) and the heat flux (\dot{Q}) along the stack. For the simplest case, assuming single plate short stack, inviscid fluid, no temperature dependence of thermophysical properties, and the thermal conductivity in x direction of both fluid and plate neglected, the above parameters allow the deduction of the added heat and acoustic power as follow:

$$\dot{Q} = -\frac{1}{2} \Pi \delta_k T_m \beta |p_1^s| |u_1^s| (\Gamma - 1) \quad (18)$$

$$\dot{W} = \frac{1}{4} \Pi \delta_k \Delta x \frac{T_m \beta^2 \omega}{\rho_m c_p} (p_1^s)^2 (\Gamma - 1) \quad (19)$$

where Π is the total perimeter of plate in contact with fluid, Δx is the stack length, and Γ is the ratio of actual temperature gradient to the critical gradient. The Γ is calculated using Eq. 20 as:

$$\Gamma = \frac{\nabla T_m}{\nabla T_{crit}} \quad (20)$$

where $\nabla T_m = \Delta T / \Delta x$. When $\nabla T_m > \nabla T_{crit}$, the heat flux is towards the pressure node and the acoustic power is positive (generated). This means that the system will be working as a prime mover. When $\nabla T_m < \nabla T_{crit}$, the heat flux is away from the pressure node and the acoustic power is negative

(consumed). This implies that the system will be working as a refrigerator. For an engine, the efficiency can be found by calculating the ratio of \dot{W} to \dot{Q} per Eq. 21 and reduced to Eq. 22 as:

$$\eta = \frac{\Delta x \beta \omega p_1^s}{\rho_m c_p u_1^s} \quad (21)$$

$$\eta = \frac{\nabla T_{crit} \Delta x}{T_m} = \frac{\nabla T_m \Delta x}{\Gamma T_m} = \frac{\Delta T}{\Gamma T_m} = \frac{\eta_C}{\Gamma} \quad (22)$$

where η_C is the maximum possible (Carnot) efficiency of an engine at T_m . Similarly for the refrigerator, the COP, which is the ratio of \dot{Q} to \dot{W} , can be described per Eq. 23 as:

$$COP = \Gamma \frac{T_m}{\nabla T_m \Delta x} = \Gamma \frac{T_m}{\Delta T} = \Gamma \times COP_C \quad (23)$$

3. Literature Review

Since the establishment of the thermoacoustic linear theory by Rott in 1980 [5], which was extended by Swift in 1988 [10], thermoacoustics have gone through a spectrum of research and development. Based on this theory, a simulation software DeltaEC (*Design Environment for Low amplitude ThermoAcoustic Energy Conversion*) was developed by Los Alamos National Laboratory (LANL) [26]. This software is still in use owing to simplicity and low computational features. The linear theory showed very good agreement with the experiments at low drive ratios (pressure amplitude over mean pressure). At large drive ratios significant deviations occurred [27]. Tijani [14] designed and extensively experimented a loudspeaker driven TAR. He proposed a general method to design and optimize a TAR system. The lowest temperature reached was -67°C, it was possible by placing the stack closer to the pressure anti-node. This was at the cost of higher cooling power and low performance. Tijani also studied the effect of lowering Prandtl number (Pr) on the performance and reported an increase in the relative coefficient of performance (COP_R). Decreasing Pr can be achieved by using mixtures of the working gases. Additionally, the plate spacing is studied and a value of 2.5 δ_k resulted in the highest cooling power, but 3.5 δ_k spacing achieved the optimal COP. On the stack design, Tasnim [28] evaluated the performance of both random porous and heterogenous stacks.

It has been concluded that the temperature difference across the stack and COP_R depend on the stack material, geometry, dimension, and position of the stack. For the sanding wave a 2 cm long stack ($\approx \lambda/50$), made of 80 PPI RVC placed at a distance of 2 cm away from the pressure antinode gives the maximum temperature difference [28]. However, best COP_R was obtained by 2.5 cm (0.025 λ) long Corning Celcor stack located at 4.25 cm ($\approx \lambda/20$) away from the pressure antinode. This means that in TARs, there are compromise between the COP_R and the maximum temperature difference. Tasnim [28] also showed that using a heterogenous stack resulted in the lowest temperature at the cold side, but at lower COP than typical homogenous stacks. As for modeling methods used in the literature, in addition to DeltaEC, SAGE which is another simulation tool is widely used [29]. While the two software are for one-dimensional (1D) study, SAGE is time formulated instead of frequency, enabling it to capture non-linear effects [30]. Finally, Computational Fluid Dynamics (CFD) allows 2D and 3D high fidelity modeling for the thermoacoustic phenomenon, with its accuracy and versatility at the cost of complexity and computational over any other modeling method.

3.1. Recent Advances In Thermoacoustic Refrigerators

Here we will present some of the recent research ideas and results of thermoacoustic refrigerators. Wang et al. [17] modeled and experimentally studied a three-unit direct-coupling heat driven traveling wave TAR operating at room temperature. The system (shown in Fig. 10) was able to achieve a cooling capacity of 3.4 kW and 4.5 kW when fed by hot heat exchanger (HHX) temperature of 300°C and 340°C, respectively. The ambient heat exchanger (AHX) temperature for both TAE and TAR was set to 50°C, while the cold heat exchanger (CHX) was kept at 10°C. The system experimentally achieved a COP of 0.19 (electrical to thermal, which includes 27% acoustic source efficiency). Wang et al. [19] proposed and modelled a novel multi-stage TAR with bypasses for the use in cascade liquefaction of natural gas. The bypasses were used to connect the regenerators to thermal buffer tube, which allowed the acoustic power to be recovered and used at the next stage. The idea of multistage cooling is to decrease the temperature gradient at each regenerator, which increases the system relative liquefaction efficiency (ratio of the theoretical minimum power consumption to the actual power consumption). For the single stage system, the temperature at CHX was 120 K, while for two stages the first CHX was at 210 K and the second was at 120 K. For three stages, the temperatures for the three successive CHXs were 240 K, 180 K, and 120 K, respectively. The proposed refrigerator reduced power consumption for the cooling of both sensible heat alone and combined with the latent heat. For combined sensible and latent heat cooling, it reduced from 9.9 kW (single-stage system) to 8.8 kW (three-stage system), corresponding to an increase of 12.6% in the relative liquefaction efficiency. For only sensible heat cooling, the acoustic power consumption was reduced from 4.9 kW (single stage system) to 3.1 kW (three-stage system), corresponding to an increase of more than 57% in the relative liquefaction efficiency. Chen and Xu [22] modelled and built a compact standing wave TAR (total length = 8 cm), which can be used for CPU cooling. The maximum temperature achieved by the cooler was 4.4°C.

Ramadan et al. [18] designed a compact TAR that is suitable for automobile applications. It was found that higher the displacement amplitude of the acoustic driver, the higher the cooling capacity of the system. The COP was lower at higher displacement amplitudes with highest attained COP of 4.0 (or 1.619 if electroacoustic efficiency is included) at 5 mm displacement amplitude, and -60° dephasing between the acoustic driver and the loudspeaker. The compactness of the system is achieved via the coaxial design alongside replacing the resonator tube by an acoustic driver at the opposite side of the loudspeaker [31]. Fig. 11 depicts such a design, where the thermoacoustic core is set in a small cylindrical cavity and surrounded by a peripheral channel. The inner acoustic driver (loudspeaker) controls the velocity, while the outer acoustic driver creates the acoustic pressure field. This design precludes the linkage between particle velocity and acoustic pressure by standing wave or travelling wave conditions. Thus, the working frequency can be set so that the wavelength is much greater than the dimensions of the resonator and the compactness of the device is thus significantly improved. The system is promising in terms of performance and compactness. Saechan and Jaworski [32] numerically studied a coaxial TAR driven by TAE. The apparatus of the system (shown in Fig. 12) is similar to a typical standing wave TAR. However, the TAR has a smaller diameter than the resonator. The annular space between the resonator and the TAR holder acts like a feedback inertance, while the space between the TAR and resonator ends acts like a compliance. This arrangement results into a compact acoustic

network that creates a local traveling wave phasing [33]. The system achieved a COP of 1.9 and overall efficiency of 22.2% (133 W cooling load was removed using 600 W heat input). This was a high efficiency compared to a similar system studied previously that reached to only 8.2%. Wang et al. [34] modelled and studied the effect of multiple stages of traveling wave refrigerator at room temperature. The temperature gradient was kept constant (313K – 237K). For a single stage traveling wave system, the highest COP (acoustic to thermal) achieved was 2.73, but with a low acoustic work utilization rate of 26%. The cooling power increased from 2.17 kW for single stage to 6.42 kW for seven stages, while the utilization rate increased from 26.5% to 82.2%. The COP reached good level at two stages, however, it was suggested that four stages would be the optimum choice due to the combined benefit of high COP (3.0), high utilization rate (60%), and high cooling power of 5.5 kW.

Sharify and Hasegawa [35] experimentally investigated a traveling wave TAR driven by a multistage traveling wave TAE as schematically illustrated in Fig. 13. The multistage for TAE helps in reducing the onset or the operational temperature. The gas oscillations started when the HHX temperature exceeded 85°C, which is relatively low. A minimum temperature of -107.4°C CHX was achieved at 270°C HHX temperature. The system achieved a very low COP (0.029). However, it was able to reach very low cooling temperatures at relatively low heating temperatures. Furthermore, Alamir [36] employed Artificial Neural Network (ANN) to predict the cooling temperature based on four parameters: frequency, stack length, position, and porosity. Other parameters were constant during the experiment. Frequency was found to be the most significant factor on the performance. The accuracy of ANN was evaluated using coefficient of determination (R^2) that was found to be 97%. The COP was calculated based on the cooling temperature, and it was very close to the measured COP which had a maximum value of 0.377. Additional review for the recent literature is summarized in Table A1 in the appendix. The recent research shows a wide variety of designs and applications of TAR that emphasize their potential to replace the current non-environment friendly cooling methods in various applications.

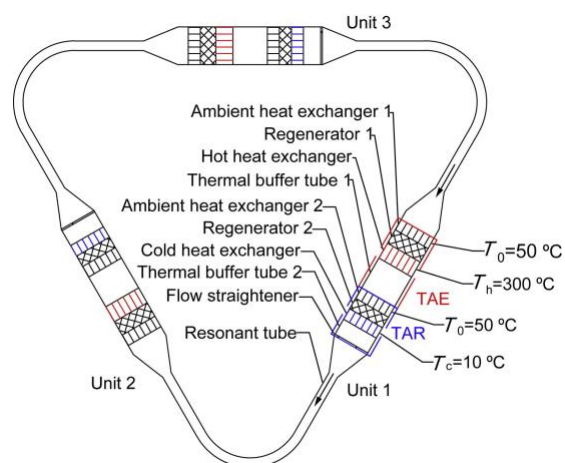


Fig. 10: Looped heat-driven TAR with direct-coupling [17]

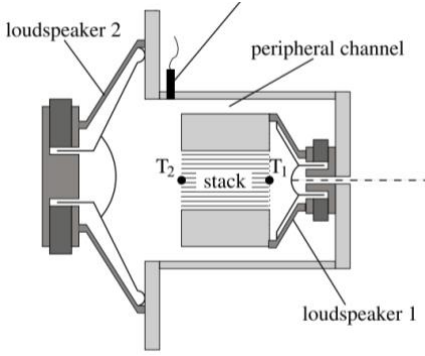


Fig. 11: Compact coaxial TAR [31]

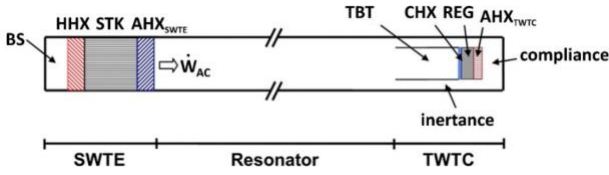


Fig. 12: Heat-driven coaxial travelling-wave TAR [32]

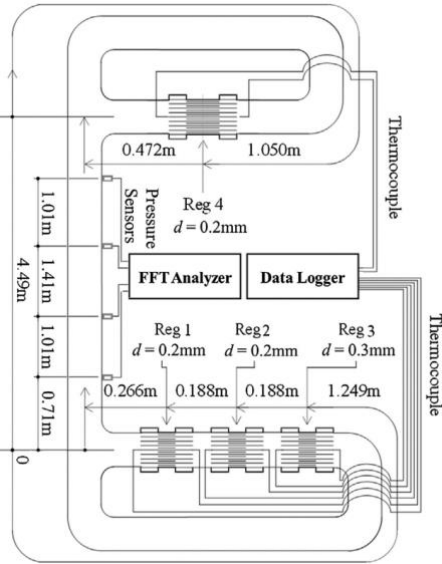


Fig. 13: Traveling-wave TAR driven by a multistage traveling-wave TAE [35]

4. Analytical Analysis

In this section, analytical method is used to analyze the influence of different parameters on performance of TAR in an attempt to construct a simple design methodology. Based on Rott's linear theory and short stack approximation, Wheatley et al. [6] derived an expression for the temperature difference along a single plate in an acoustic standing wave. Atchley et al. [27] modified the equation to include the thermal conductivity of the fluid. The derivation of the equation is given in the attached Appendix at the end. The expression is written per Eq. 24 as:

$$\Delta T = \left(\frac{1}{4 \rho_m a [(K_p l + K_g y) / \Delta x] (1 + \sigma)} \frac{p_0^2 \delta_k (1 + \sqrt{\sigma}) \sin 2kx}{\rho_m \Delta x T_m \omega (\gamma - 1) (1 - \sigma^2)} \right)^{-1} \times \left(1 + \frac{1}{4 [(K_p l + K_g y) / \Delta x] \rho_m \Delta x T_m \omega (\gamma - 1) (1 - \sigma^2)} \frac{p_0^2 \delta_k (1 - \sigma \sqrt{\sigma})}{\rho_m \Delta x T_m \omega (\gamma - 1) (1 - \sigma^2)} (1 - \cos 2kx) \right)^{-1} \quad (24)$$

where K_p is the plate thermal conductivity, γ is the ratio of isobaric to isochoric specific heats (c_p/c_v), and x is the stack's center position. Several important assumptions are made to arrive to Eq. 24 including $\Delta x \ll \frac{\lambda}{2\pi}$, $\delta_k, \delta_v \ll d_g$, and $\Delta T \ll T_m$. This implies that stack is short enough to avoid the perturbation of the acoustic wave, the spacing between the plates is relatively large compared to the thermal/viscous penetration depth, and the temperature gradient along the stack is much smaller than the mean temperature. Furthermore, the plate heat capacity per unit area is much greater than gas heat capacity per unit area. Atchley et al. [27] validated Eq. 24 experimentally at different drive ratios and mean pressures. Discrepancies arose as drive ratio increased beyond 1.1% at mean pressure near 114 kPa. However, as the mean pressure increased, the discrepancies occurred at lower drive ratios. Also, the location where the maximum temperature difference occurred was approximately the same even at relatively high drive ratios (e.g., 1.99%).

To gain more insight to this expression and reveal its limits, comparison to different experimental results from literature is done. Shivakumara and Arya [37] experimentally studied the effect of drive ratio, mean pressure, and plate spacing on the performance of the TAR. At drive ratio of 0.6% and mean pressure of 200 kPa, the result from the analytical equation (28.66 °C) is close to the result obtained from the experiments (~23 °C). It should be noted that the experimental result is measured at cooling load of 2 W, which reduces the temperature difference. Obviating the cooling load would achieve a higher temperature difference experimentally, which means a closer value to the one obtained analytically. At higher drive ratios (1% and 1.6%), the temperature difference grows both analytically and experimentally, however, the error becomes much larger. Similarly, at higher mean pressure (400 kPa and 600 kPa), the discrepancy is noticeably large even at a drive ratio of 0.6%. As for the increasing plate spacing, both analytical and experimental results showed a decrease in temperature difference and with good agreement on the values.

Saechan and Dhuchakallaya [38] experimentally investigated the effect of stack length on the temperature difference. Three stack lengths (with the ratio of stack length to resonator length shown in the parentheses) were tested; 5 cm (4%), 8 cm (6.6%), and 11 cm (9%). At 5 cm stack length and stack position of 10 cm, the analytical and experimental temperature differences were 16°C and 11°C, respectively. A longer stack resulted in larger difference between the experiments and the analytical results. Moreover, experimentally, the highest temperature difference was obtained for the 8 cm stack length, while it was for the 11 cm stack analytically. It is worth noting that, a longer stack will always yield higher temperature difference analytically, which is not the case in real systems where there is an optimum stack length [14, 39]. This emphasizes the importance of remembering short stack assumption in the analytical equation. It should be noted that the drive ratio of the system was 1.5% and the stack used in the experiments is circular pore stack that was hand made from thermoplastic pipes. This might be the reason for incurring high error at relatively short stack (e.g., 8 cm), and knowing the derived equation limitation for parallel plate geometry at low drive ratios. Regarding the frequency, varying the frequency away from the resonance frequency has almost no effect on the temperature difference, analytically. However, realistically, operating far away from the resonance frequency significantly decreases the pressure amplitude that in turn decreases the temperature difference. Comparing the analytical results to the experimental results from Kajurek et al. [40] shows a great agreement when

operating at the resonance frequency, while discrepancies grow as frequency moves away from the resonance. Because thermoacoustic systems always operate close to resonance frequency the frequency factor is unimportant parameter.

Given the above analytical and experimental literature comparison, initial design guidelines can be drawn to achieve comparable analytical experimental results. These are: stack length $\leq 5\%$ of the resonator length, drive ratio $\leq 2\%$ of the mean pressure, mean pressure $\leq 200\text{kPa}$, and a stack made of parallel plates. Nevertheless, slight deviating from these values would still give reasonable accuracy.

4.1. Effect Of The Parameters (Case Study)

To study the effect of varying different parameters on the performance of a TAR, it is assumed that we have a one-meter long resonator representing quarter wavelength with a parallel plate stack 5 cm-long (5% of the resonator) at plate spacing of $3\delta_k$. The working fluid mean temperature stays at the ambient, i.e., 300 K. Several parameters will be varied including: the drive ratio, mean pressure, stack conductivity, and the working fluid. This will be done by varying single parameter while keeping other parameters fixed. We will adopt left to right axial coordinate for the resonator sitting at $x = 0$ value where the closed end (pressure antinode) is located.

4.1.1. Drive Ratio

It is assumed that the system has air at atmospheric pressure as working fluid, and the thermal conductivity of the stack is 1 W/m.K. Fig. 14 shows the effect of drive ratio on the temperature difference at different stack positions. It is obvious that increasing drive ratio increases the maximum temperature difference. It also shifts the optimal stack position closer to pressure antinode. However, increasing the drive ratio in the analytical equation (Eq. 24) will always increase the temperature difference, which is not realistic. At high drive ratios, non-linear effect grows that undermines the predicted performance by the linear theory.

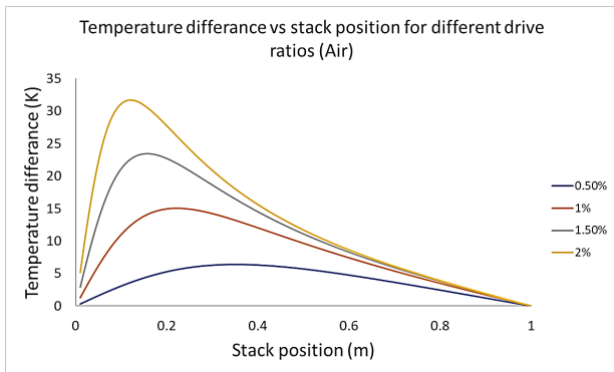


Fig. 14: Effect of drive ratio on TAR performance

4.1.2. Mean Pressure

Fig. 15 depicts the effect of varying mean pressure while maintaining the drive ratio at 0.5% and other system parameters fixed. It is obvious that the increase in mean pressure increases the temperature difference. In fact, it displays similar effect to the drive ratio as they are both linearly related. However, the mean pressure can also affect the fluid properties. One of the critical properties that is affected by the mean pressure is the thermal penetration depth. Increasing the mean pressure decreases the thermal penetration depth. Analytically, lower

penetration depth implies lower temperature difference. Additionally, the decrease in thermal penetration depth results in decreasing the required spacing between the plates, which also decreases the required plate thickness to keep the blockage ratio (porosity) constant. This suggests that at extremely high mean pressure values, additional manufacture constrains are imposed on the plate thickness and spacing.

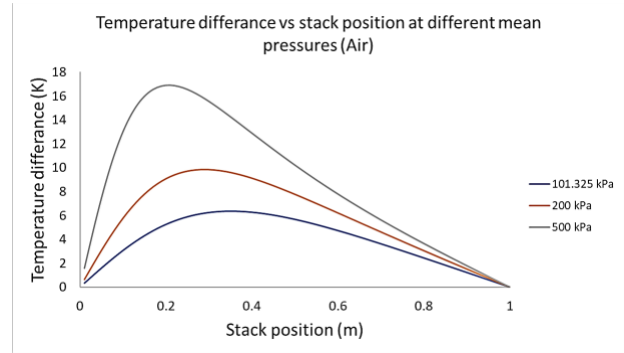


Fig. 15: Effect of fluid mean pressure on TAR performance

4.1.3. Stack Conductivity

Fig. 16 shows the effect of varying the thermal conductivity on the temperature difference of the TAR. Other conditions are constant (drive ratio of 1% with air as working fluid at atmospheric pressure). It can be clearly noticed that temperature difference increases at lower stack thermal conductivity. This agrees with Swift's work where it is suggested to use stack with low thermal conductivity and high heat capacity [1]. Also, the optimal stack position shifts closer towards pressure antinode at lower thermal conductivity.

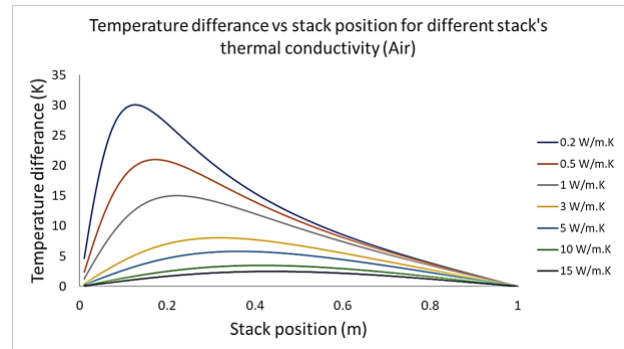


Fig. 16: Effect of thermal conductivity of stack on TAR performance

4.1.4. Working Fluid

The temperature difference for three fluids at atmospheric pressure were also deployed in the thermoacoustic system. The other system parameters were fixed, including 1% drive ratio and stack with thermal conductivity of 1 W/m.K. Results are depicted in Fig. 17. It shows that Helium achieved the highest maximum temperature difference, followed by Hydrogen, and then Air. This is mainly due to the lower value of Pr of the Helium followed by Hydrogen then the Air [14]. Lower Pr means that the ratio of the viscous penetration depth (δ_v) to the thermal penetration depth (δ_k) is lower. This is in fact preferable because it means that the undesirable viscous effects are less significant compared to the desirable heat dissipation effects. Another interesting result from this figure is that the optimum stack position for the Hydrogen is a bit closer to the pressure antinode compared to Air and Helium.

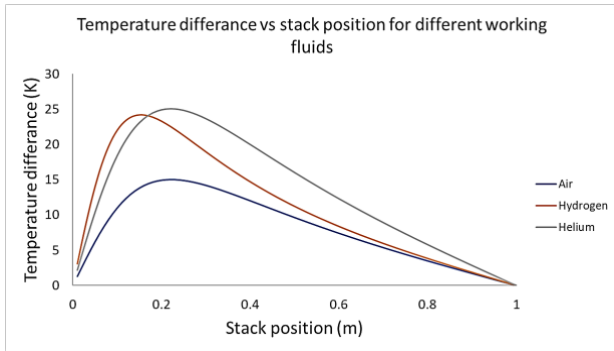


Fig. 17: Effect of working fluid on TAR performance

5. Future Prospect of TARs

Typically, TARs, especially standing wave type, have simple designs, and are easy and inexpensive to manufacture. The resonator needs to withstand the temperature variations, and it is usually insulated to minimize heat losses. Stainless steel and thermoplastic materials (e.g., PVC and acrylic) are commonly used for the resonator. As for the regenerator, the heart of the of the TA device, it can be made of material of low conductivity and high heat capacity. Some typical materials are plastics (e.g., Mylar or Kapton sheets), steel, and ceramics. The aforementioned materials are widely available and typically inexpensive. As for traveling wave systems, they usually have more complicated designs, such as looped or toroidal designs. However, they can attain higher efficiencies. The stack is usually made of plain-weave metal screens [1]. This ensures the perfect thermal contact required by traveling wave systems. One manufacturing technique that seems promising is 3D printing. It was found by Zolpakar et al. [39] that a 3D printed stack outperformed typical Mylar sheets and Celcor ceramic stacks. The wide availability of 3D printing can aid in lowering the cost of TARs.

TAR design variations render their potential in many applications. For instance, miniaturized TARs that operate at ultrasonic frequencies resulted in coolers that are suitable for electronics [23]. Furthermore, TARs can work at very low temperatures. The TAR built by Tijani [14] was able to achieve a CHX temperature of -67°C . Another system was able to achieve -107°C [35]. Hence lower temperatures can be also pursued for Cryogenics applications, such as natural gas liquefaction. Moreover, compact designs can also enhance TARs potential for automobile applications [18].

There is no dispute that TAR efficiency is still low to compete with current cooling methods. In standing wave systems the necessity of poor thermal conductivity in stack significantly lowers the performance. This calls for improving other system components to enhance the overall efficiency. Another aspect in improving system design is the acoustic power source. Loudspeakers which typically used are extremely inefficient in electrical to acoustical power conversion. One alternative is the usage of TAE and TAR in tandem. TAE also operates at low efficiency, yet can compensate that by utilizing waste heat or solar energy and rendering system sustainability. Additionally, the coupling of TAE to TAR allows to use multistage and/or looped designs to improve the efficiency of the system.

Despite the wealth of literature to improve TARs performance, more advancements in terms of design and optimization are needed. This means that it is necessary for researchers to explore

novel strategies to design TARs. Moreover, nowadays, the advancements in manufacturing techniques allow for further research and improvements in TARs manufacturing, especially for the stack. Additionally, non-linear phenomena that occurs in TA systems is still less researched and described. All in all, TARs have very good potential in terms of reliability, inexpensiveness, and application versatility and that is still opening a wide door of research in improving this technology.

6. Conclusion

Thermoacoustic systems can be classified into two types: thermoacoustic engine (TAE), and thermoacoustic refrigerator (TAR). In general, Thermoacoustic systems are reliable due to the absence of moving parts. TAE is capable of recycling waste heat or harnessing solar power, which makes it sustainable. As for TAR, contrary to conventional refrigeration systems, it utilizes environment-friendly gases (e.g., Air and Helium). Additionally, the recent developments in TARs show wide variety of designs and applications. This boosts their potential to replace the current cooling methods in many applications. Analytical simulation was performed to find the temperature difference across a stack depending on various operating conditions. The analytical equation was validated against experimental data in the literature. A Case study was carried out with the initial guidelines as: stack length $\leq 5\%$ of the resonator length, drive ratio $\leq 2\%$ of the mean pressure, mean pressure $\leq 200\text{kPa}$, and a stack made of parallel plates. Within these limits, the effect of drive ratio, mean pressure, stack conductivity, and working fluid was studied. The temperature difference increased with increasing drive ratio or mean pressure. Lower thermal conductivity of the stack resulted in higher temperature differences. Furthermore, fluids with lower Prandtl number performed better than their counterparts.

Nomenclature

a	Speed of sound in fluid
B	Blockage ratio (porosity)
c_p	Specific heat
COP	Coefficient of Performance
D	Drive ratio
f	Frequency
h	Enthalpy
\dot{H}_2	Total energy flux
k	Wave number
K	Thermal conductivity
l	Thickness of plate
M	Mach number
T	Temperature
p	Pressure
\dot{Q}	Heat flux
s	Entropy
t	Time
u, v	Velocity/ Velocity vector
Re	Real part
\dot{W}	Work flux/acoustic power
x	Stack's center position
y	Spacing between plates
Δx	Stack length
<i>Greek Symbols</i>	
μ	Dynamic viscosity
γ	Ratio of isobaric to isochoric specific heats
σ	Prandtl number
σ'	Stress tensor

ρ	Density
β	Thermal expansion coefficient
ω	Angular frequency
δ_k	Thermal penetration depth
δ_v	Viscous penetration depth
ξ	Displacement amplitude
Π	Perimeter
Γ	Normalized temperature gradient
λ	Wave length
η	Efficiency
ϕ	Phase angle

Subscripts and Superscripts

0	Amplitude
1	Complex oscillating/ first order
2	Second order
c	At cold heat exchanger
C	Carnot
g	Fluid
H	At hot heat exchanger
m	Mean value
p	Solid (plate)
R	Relative to Carnot
s	Standing wave

Appendix

In this section, the derivation of Eq. 24 is presented. It will be assumed that the stack is parallel-plate and short (does not perturb the sound wave). Also, the spacing between the plates is assumed to be much larger than δ_k , so the boundary-layer approximation applies [6]. The x -axis is in the direction of sound propagation, while the y -axis is normal to solid-fluid boundary where y is the distance from the boundary ($y = 0$). In this analysis, all components in z -direction will be neglected. Starting with Rott's acoustic approximation of the oscillating variables [5]:

$$p = p_m + Re[p_1(x)e^{i\omega t}] \quad (A1)$$

$$u = Re[u_1(x, y, z)e^{i\omega t}] \quad (A2)$$

$$T = T_m(x) + Re[T_1(x, y, z)e^{i\omega t}] \quad (A3)$$

$$\rho = \rho_m(x) + Re[\rho_1(x, y, z)e^{i\omega t}] \quad (A4)$$

The general equation of heat transfer for fluids is expressed per Eq. A5 as [41]:

$$\rho T \left(\frac{\partial s}{\partial t} + v \cdot \nabla s \right) = \nabla \cdot K \nabla T + (\sigma' \cdot \nabla) \cdot v \quad (A5)$$

$$ds = -\frac{\beta}{\rho} dp + \frac{c_p}{T} dT \quad (A6)$$

Substituting Eq. A6 into Eq. A5, where $\frac{\partial s}{\partial t} + v \cdot \nabla s = \frac{ds}{dt}$:

$$-T\beta \frac{dp}{dt} + \rho c_p \frac{dT}{dt} = \nabla \cdot K \nabla T + (\sigma' \cdot \nabla) \cdot v \quad (A7)$$

where $\beta = \frac{1}{T}$ for ideal gases. Substituting the oscillating variables (Eq. A1 through Eq. A4) into Eq. A7, while neglecting second-order terms, replacing the time derivatives ($\delta/\delta t$) by $i\omega$, and ignoring conduction of fluid in x -direction leads to:

$$-i\omega p_1 + \rho_m c_p \left(i\omega T_1 + u_1 \frac{dT_m}{dx} \right) = K \left(\frac{\partial^2 T_1}{\partial y^2} \right) \quad (A8)$$

where, u_1 is a function of x and y which can be described using Eq. A9 [5]:

$$u_1(y, x) = u_1(x) \left[1 - e^{-\frac{(1+i)y}{\delta_v}} \right] \quad (A9)$$

To avoid confusion between $u_1(x)$ and $u_1(x, y)$, the former will be replaced by u_∞ . Rewriting Eq. A9:

$$u_1 = u_\infty \left[1 - e^{-\frac{(1+i)y}{\delta_v}} \right] \quad (A10)$$

Substituting Eq. A10 in Eq. A8 and solving for $T_1 = 0$ at $y = 0$, and T_1 is finite at $y = \infty$. The result is Eq. A11 [5]:

$$T_1 = \frac{p_1}{\rho_m c_p} \left(1 - e^{-\frac{(1+i)y}{\delta_k}} \right) + \frac{dT_m}{dx} \frac{i}{\omega} u_\infty \left(1 + \frac{\sigma}{1-\sigma} e^{-\frac{(1+i)y}{\delta_v}} - \frac{1}{1-\sigma} e^{-\frac{(1+i)y}{\delta_k}} \right) \quad (A11)$$

Considering that:

$$\eta = \frac{(1+i)y}{\delta_v} \quad (A12)$$

$$\eta' = \frac{(1+i)y}{\delta_k} \quad (A13)$$

$$\theta = \frac{dT_m}{dx} \frac{1}{T_m} \quad (A14)$$

Multiplying both sides of Eq. A11 by $\rho_m c_p$, and using Eq. A12, Eq. A13, Eq. A14. Eq. A11 can be rewritten:

$$\rho_m c_p T_1 = p_1 (1 - e^{-\eta'}) + \theta \rho_m c_p T_m \frac{i}{\omega} u_\infty \left(1 + \frac{\sigma}{1-\sigma} e^{-\eta} - \frac{1}{1-\sigma} e^{-\eta'} \right) \quad (A15)$$

Replacing $c_p T_m$ by $\frac{a^2}{\gamma - 1}$, and rearranging the equation:

$$\rho_m c_p T_1 - p_1 = -p_1 e^{-\eta'} + \frac{i \rho_m a^2 \theta}{\omega} \frac{1}{\gamma - 1} \frac{1}{1 - \sigma} u_\infty (1 - e^{-\eta'}) - \frac{i \rho_m a^2 \theta}{\omega} \frac{\sigma}{\gamma - 1} \frac{1}{1 - \sigma} u_\infty (1 - e^{-\eta}) \quad (A16)$$

As for the axial total energy flow in the gas, it is described using Eq. A17 [6]:

$$\overline{H}_2 = \Pi \int dy (\overline{\rho u h}) \quad (A17)$$

where, the bar indicates time average. Knowing that [1]:

$$s_1 = -\frac{p_1}{\rho_m T_m} + \frac{c_p T_1}{T_m} \quad (A18)$$

$$h_1 = c_p T_1 \quad (A19)$$

Substituting Eq. A1, Eq. A2, Eq. A18, Eq. A19 in Eq. A17:

$$\overline{H}_2 = \Pi \int dy (\rho_m T_m \overline{s_1 u_1} + \overline{p_1 u_1}) \quad (A20)$$

The first term in Eq. A20 is the heat flow (\overline{Q}_2), which is our interest, while the second term is the work flow (\overline{W}_2). Substituting Eq. A18 in the first part of Eq. A20 gives:

$$\overline{Q}_2 = \Pi \int dy (\overline{\rho_m c_p T_1 - p_1}) u_1 \quad (A21)$$

To solve Eq. A21, firstly substituting Eq. A 10 and Eq. 16 in Eq. A21. Then, defining the phase ϕ of velocity u_∞ with respect to pressure p_1 by taking u_∞ to be $u_\infty e^{i\phi}$ explicitly, and using the fact that $\overline{ab} = \frac{1}{2} Re(\tilde{a}\tilde{b})$, where the tilde indicates complex conjugate, and a and b are arbitrary complex variables. The result is [6]:

$$\overline{Q}_2 = -\frac{\Pi}{4} u_\infty p_1 \delta_k \left(\frac{1-\sqrt{\sigma}}{1+\sigma} \cos\phi - \frac{1+\sqrt{\sigma}}{1+\sigma} \sin\phi \right) - \frac{\Pi}{4} u_\infty^2 \delta_k \frac{\rho_m a^2 \theta}{\omega(\gamma-1)} \frac{1-\sigma\sqrt{\sigma}}{1-\sigma^2} \quad (A22)$$

Since it was assumed that the stack is short and doesn't perturb the wave, u_∞ and p_1 are expressed per Eq. A23 and Eq. A24, respectively as:

$$p_1 = p_0 \cos(kx) \quad (A23)$$

$$u_\infty = \frac{p_0}{\rho_m a} \sin(kx) \quad (A24)$$

Also, for a standing wave:

$$\phi = -\frac{\pi}{2} \quad (A25)$$

Substituting Eq. A23, Eq. A24, and Eq. A25 in Eq. A22 gives:

$$\overline{Q_2} = \frac{\pi \omega p_0^2}{4 \gamma \rho_m} \delta_k \left[\frac{1+\sqrt{\sigma}}{1+\sigma} \left(\frac{a}{2\omega} \right) \sin \left(\frac{2\omega x}{a} \right) + 2 \frac{1-\sigma\sqrt{\sigma}}{1-\sigma^2} \frac{\theta}{(\gamma-1)} \left(\frac{a}{2\omega} \right)^2 \left(1 - \cos \left(\frac{2\omega x}{a} \right) \right) \right] \quad (A26)$$

Neglecting heat transfer between the stack and surroundings, the heat transfer in the system is described per Eq. A27 as:

$$\overline{Q_2} - K_p A \frac{dT}{dx} = 0 \quad (A27)$$

Inserting Eq. A26 in Eq. A27, and integrating over the stack length (Δx) gives:

$$\Delta T = \left(\frac{1}{4 \rho_m a [(K_p l)/\Delta x] (1+\sigma)} \frac{p_0^2 \delta_k (1+\sqrt{\sigma})}{\sin 2kx} \right) \times \left(1 + \frac{1}{4 [(K_p l)/\Delta x] \rho_m \Delta x T_m \omega (\gamma-1) (1-\sigma^2)} \frac{p_0^2 \delta_k (1-\sigma\sqrt{\sigma})}{(1-\cos 2kx)} \right)^{-1} \quad (A28)$$

This equation is identical to Eq. 24, except for one term which is $K_p l/\Delta x$. By modifying this term to $(K_p l + K_g y)/\Delta x$ so it includes the thermal conductivity of fluid, the equation takes the form of Eq. 24:

$$\Delta T = \left(\frac{1}{4 \rho_m a [(K_p l + K_g y)/\Delta x] (1+\sigma)} \frac{p_0^2 \delta_k (1+\sqrt{\sigma})}{\sin 2kx} \right) \times \left(1 + \frac{1}{4 [(K_p l + K_g y)/\Delta x] \rho_m \Delta x T_m \omega (\gamma-1) (1-\sigma^2)} \frac{p_0^2 \delta_k (1-\sigma\sqrt{\sigma})}{(1-\cos 2kx)} \right)^{-1} \quad (24)$$

Table A1. Literature review of recent papers in TAR

Researchers	Wave type	Source of acoustic power	Stack/ Regenerator	Tube/ Resonator	Application	Experimental/ Simulation	Heat exchangers	Working fluid/ Operating conditions	Major findings
Abd El-Rahman et al. [42]	Standing Wave	Two out of phase reciprocating pistons (rotary mechanism)	30 cm-long stack (simple porous ceramic material ;100-CPSI)	30-cm-long acrylic resonator fitted with two 90° bends.	Compact refrigerator	Both Model using DeltaEC	No heat exchangers	Air at ambient conditions Drive ratio: 7% Frequency: 42 Hz	<ul style="list-style-type: none"> Electro-acoustic efficiency of the rotary mechanism is 0.2%. Maximum temperature difference of 27 °C at 180 degrees phasing. Carnot COP of 11. Remarkable discrepancies between experimental data points and DeltaEC values caused by significant non-linear losses, such as flow streaming and potential turbulence.
Shivakumara and Arya [37]	Standing Wave	Loudspeaker	Parallel plate stack made of Mylar sheets enclosed by aluminium sleeve (aluminium is used only to create a cylinder opened from two ends to hold the Mylar sheets).	Resonator made of PVC	-	Experimental	Both heat exchangers made of hollow copper tube, and covered with copper mesh with porosity of 0.72	Zero air (contains less than 0.1 ppm of hydrocarbons)	<ul style="list-style-type: none"> The paper studied the effect of varying the following parameters: frequency, drive ratio, mean pressure, stack's parallel plates spacing, and cooling load. Lower spacing values corresponded to higher COP and temperature difference values. Higher drive ratio increases the temperature difference but lowers the COP. Higher cooling loads decrease the temperature difference, but increases the COP. Higher mean pressure increases both the COP and the temperature difference. Highest COP was 1.619, while highest temperature difference was 30.77°C.
Xiao et al. [21]	Standing wave	-	Stainless steel stack	-	Electronics cooling	Simulation using COMSOL	Copper heat exchangers	Helium Temperature: 298 K Frequency: 100 Hz	<ul style="list-style-type: none"> A novel method of cooling by combining thermoacoustic heat dissipation effect with oscillating convection was proposed. The convection only cooling mechanism performed better than the proposed coupled cooling method. However, at low stack length, and at the same velocity magnitude, the proposed cooling method performed better.
Rahman and Zhang [43]	Standing wave	Loudspeaker	-	-	-	Optimization using fruit fly optimization algorithm (FOA)	-	Helium Pressure: 10 bar Temperature: 250 K	<ul style="list-style-type: none"> This paper investigated the optimization of both COP and cooling power using FOA. The optimized parameters are length and position of the stack, blockage ratio, and drive ratio. The optimized COP had a value of 1.83 compared to 1.58 in a previous result. However, attaining this high COP decreased the cooling power of the system (1.041 W).
Chen et al. [44]	Hybrid	Two acoustic drivers at constant displacement amplitude of 0.001 m. They operate at the same frequency	Carbon steel parallel plates with 0.0001 m thickness and spacing. It is placed in the middle of the tube.	0.5 m-long, and 0.02 m diameter duct	--	Modelling	-	Air at atmospheric pressure and temperature	<ul style="list-style-type: none"> The paper modelled a thermoacoustic refrigerator with two acoustic drivers. Depending on the frequency of the drivers and the phasing, the wave through the stack/regenerator can be pure standing wave, pure traveling wave, or a hybrid between them. At phasing angle of 90°, the maximum temperature difference of almost 30 K occurred at a frequency of 282 Hz and 302 Hz. The former had positive temperature gradient, while the later had negative temperature gradient. The wave at both frequencies is hybrid. Generally, the maximum temperature gradient increases with the increase of the phasing angle.
Wang et al. [45]	Traveling wave	Heat generated acoustic power (TAE)	Regenerator made of 120-mesh stainless steel screens, with length of 45 mm for TAE, and 35 mm for TAR. Both has 110 mm diameter.	3000 mm long, 28 mm diameter resonator tube between each two subunits	Room temperature refrigeration	Both Modelling using SAGE software	Shell-tube heat exchangers, with 0.15 porosity, and 1 mm tube diameter	Helium at 10 Mpa Frequency: 56 Hz	<ul style="list-style-type: none"> The paper proposed a looped multistage heat driven thermoacoustic refrigerator with direct coupling between the TAE and TAR. At a certain cooling temperature, there is an optimum heating temperature for the direct coupling heat driven TAR. Up to 5 stages were simulated. It was found the two-stage system had the highest COP, while the four-stage system had the highest cooling capacity (2.2 kW for each stage). There was a large deviation between all experiments and calculations (almost 50%). In all cases, the COP and the cooling capacity increased with increasing the CHX temperature. Replacing the flow straightener at the outlet TAR with elastic diaphragm increased the COP and the cooling capacity.
Chi et al. [46]	Traveling wave	Heat generated acoustic power (TAE)	Screen mesh of 88% porosity, and 38 µm wire diameter	U-type gas liquid resonator between each two subunits.	Room temperature refrigeration	Simulation using SAGE software	Shell-tube heat exchanger with 20% porosity	Helium And the liquid in the resonator is water	<ul style="list-style-type: none"> The paper studied different working gases in a gas-liquid multistage coupled heat driven TAR. Four working gases were tested; helium, hydrogen, nitrogen, and argon. The system utilizes a U-shaped tube, which enhances the system compactness. The highest cooling capacity of 4557 W was achieved by hydrogen at 10 Mpa. The highest COP (thermal to thermal) of 0.71 was achieved by hydrogen at 1 Mpa.
Widyaparaga et al. [47]	Hybrid	Loudspeaker (Jordan JX92S full range woofers)	30 mm-long regenerator made of stainless steel mesh (150 meshes). Mesh opening has a width and height of 0.1 mm. The regenerator was positioned in the centre of the device	Half wavelength resonator made of acrylic tube with length of 660 mm	-	Experimental	-	Air at atmospheric conditions Frequency: 260 Hz	<ul style="list-style-type: none"> The paper studied the alteration of heat pumping direction by varying the magnitude and phase difference of two acoustic drivers. The variation of magnitude was investigated by changing the power of one speaker while keeping the other speaker's power at maximum (23 W). The phase angle between the speakers was kept to zero.
Zolpakar et al. [39]	Standing wave	Loudspeaker (PRIME R14X2)	3D printed stack with spacing of 0.5 mm and thickness at 0.5 mm. The material is VeroWhitePlus Rgd835 (thermal	Quarter-wavelength resonator tube with inner diameter of 34	-	Experimental	-	Air at atmospheric conditions Frequency: 400 Hz	<ul style="list-style-type: none"> The paper studied the usage of 3D printed stacks instead of the conventional Mylar or Celcor ceramic stacks. The stack length of 4 cm and at center position of 5 cm corresponded to the lowest cold temperature of 18.9°C, and the highest temperature difference of 18.1°C. The 3D printed stack performance in terms of both temperature difference and lowest temperature was better than Celcor Ceramic and Mylar stacks under same operating conditions studied by the same author in previous study.

			conductivity: $k = 0.23 \text{ Wm}^{-1}\text{K}^{-1}$ and specific heat of $1000 \text{ Jkg}^{-1}\text{K}^{-1}$)	mm and length of 21 cm					
Rahpeima and Ebrahimi [48]	Standing wave	No acoustic driver (it is just simulation, so the oscillations were modelled)	Parallel plate stack	Half-wavelength resonator tube with length of almost 5 m	-	Simulation using COMSOL	Copper heat exchangers	Helium at 10 kPa and 293 k. Frequency: 100 Hz Drive ratio: 1.7%	<ul style="list-style-type: none"> The paper studied the effect of changing different geometrical and thermophysical parameters on the TAR performance. Increasing the plate thickness decreased the temperature difference, but increased the COP. The optimum spacing between the plates was $3.33\delta_k$. Increasing the heat capacity of stack increased the time the TAR needs to reach steady state. Decreasing stack thermal conductivity resulted into increasing the temperature difference but decreasing the COP.
Elaziz et al. [49]	Standing wave	Speaker	Stack fabricated from thermoplastic material	Quarter-wavelength resonator	-	Comparing Adaptive Neuro Fuzzy Inference System (ANFIS) results with experiments	Finned-tube heat exchanger	Helium	<ul style="list-style-type: none"> The paper studied the usage of ANFIS based on Crow Search Algorithm (CSA) method to predict the oscillatory heat transfer coefficient (OHTC) outside the heat exchangers of TAR. The frequency of oscillation and mean pressure value were chosen to be the inputs to the ANFIS-CSA model, as they were proved in previous studies as the most significant features affecting the OHTC. The ANFIS-CSA model showed high accuracy in predicting the OHTC at all experiments ($R^2 = 0.9835$. RMSE=0.0065, and MSE=0.0425E-3).
Gökay and Karabacak [50]	Standing wave	Speaker (JVC CS-J420X)	10 cm-long circular pores stack made of Polypropylene pipettes ($k=0.15 \text{ W/mK}$).	Quarter-wavelength resonator with one open end.	-	Experimental	-	Air	<ul style="list-style-type: none"> The paper studied the effect of changing the sound wave type on the temperature difference along the stack at three resonator diameters (50 mm, 70 mm, and 100 mm). The wave types are Sine, Square, Triangular, Sawtooth, and Trapezoidal. The resonance frequency changed based on the wave type. At 50 mm diameter, the Sine wave attained the highest temperature difference of 24.61°C. At 70 mm diameter, the Sawtooth wave attained the highest temperature difference of 21.97°C. At 100 mm diameter, the Trapezoidal wave attained the highest temperature difference of 20.54°C.
Widyaparaga et al. [51]	Hybrid	Loudspeaker (Jordan JX92S full range woofers)	30 mm-long regenerator made of stainless steel mesh (150 meshes). The regenerator was positioned in the centre of the device.	Half wavelength resonator made of acrylic tube with length of 1730 mm, inner diameter of 50 mm.	-	Experimental	-	Air at atmospheric conditions Frequency: 100Hz	<ul style="list-style-type: none"> The paper studied acoustic field alteration in a straight tube using dual acoustic driver at 100 Hz. The system achieved largest temperature difference of 23.6°C when the speaker power is 17% of the other speaker power.
Xu et al. [52]	Traveling wave	Heat generated acoustic power (TAE)	Woven screen regenerator TAE regenerator: 80% in porosity, 150- mesh, $52 \mu\text{m}$ in wire diameter TAR regenerator: 70% in porosity, 300-mesh, $31 \mu\text{m}$ in wire diameter	No resonator	Natural gas liquefaction	Simulation using SAGE software	HHX: plated-fin heat exchanger AHX (TAE): shell-tube heat exchanger AHX (TAR): plated-fin heat exchanger working fluid. CHX: plated-fin heat exchanger	Working gas was not mentioned in the paper Frequency: 50 Hz Pressure: 35 bar	<ul style="list-style-type: none"> The paper proposes a novel method of low temperature cooling. The system is multistage heat-driven piston coupled thermoacoustic-Stirling cooler. The system consists of compressor, three TAEs, two TARs, four piston-cylinder assemblies, and a phase shifter assembly (inertance tube and gas reservoir). The relative Carnot efficiency of the TAEs is 63.5%. The relative Carnot efficiency of the TARs is 36.8%. The thermal to cooling exergy efficiency is 23.4%. Compared to similar systems in the literature. This efficiency is higher by 60%. Additionally, the cooling capacity of this system is higher by 80%.
Harikumar et al. [53]	Standing wave	Loudspeaker	Stack made of plastic straws glued together	0.96 m-long square duct	-	Experimental	-	Air at atmospheric conditions Frequency: 70 Hz	<ul style="list-style-type: none"> The paper tests the performance of TAR in a square duct resonator. The stack positioned in the middle had higher temperature difference than the stack close to the closed end of the duct.
Wang et al. [54]	Traveling wave	Heat generated acoustic power (TAE)	TAE regenerator: 35 mm-long TAR regenerator: 25 mm - long No information about the materials were given	A resonator tube between each TAE and TAR.	-	Simulation using SAGE software	HHX: heat source AHX: reject heat to circulating water	Helium at 10 Mpa Frequency: 63.5 Hz	<ul style="list-style-type: none"> The paper proposed a novel looped low-temperature heat-driven thermoacoustic refrigerator. The system consists of two TAEs and two TARs, where a resonator tube connect between them to form a loop. The system achieved a cooling power of 3102 W, COP (thermal to thermal) of 0.41 and overall relative Carnot efficiency of 13.4%. At the same CHX temperature, increasing the pressure increased both the cooling power and the efficiency. At same CHX temperature, higher HHX temperatures yielded to higher cooling powers. At each HHX temperature, the maximum efficiency occurred at different CHX temperature.
Yahya et al. [55]	Standing wave	Loudspeaker	Different random and parallel plate stacks were tested. All stacks are 150 mm-long.	Half-wavelength square duct resonator with a length of 1.82 m.	-	Experimental	AHX: made of array of brass fins and flow passages for water to flow. CHX: electrical heater.	Air at atmospheric conditions Frequency: 72 Hz	<ul style="list-style-type: none"> The paper studied the performance of random stack materials in TAR. Random stacks are usually inexpensive to manufacture, and sometimes can be found as waste material. Random stack made of steel wool achieved a COP, relative COP, and temperature difference of 0.21, 0.13%, and 7.2°C, respectively. Mylar sheets stack had better performance than all random stacks.

Chen and Xu [56]	Standing wave	Two acoustic drivers at constant displacement amplitude of 0.001 m.	Porous material made of parallel carbon steel plates with length of 0.1 m, spacing of 0.001 m, and plate's thickness of 0.001.	1 m-long looped tube with 0.02 m diameter.	-	Modelling based on the linear theory	Heat exchangers made of parallel copper plates	Air at atmospheric conditions	<ul style="list-style-type: none"> • The paper studied the heat transport in a porous material inside a looped-tube dual-acoustic driver TAR. • The dual acoustic driver mechanism allows an active control for the TAR by changing the phasing between the acoustic driver or changing the acoustic drivers position. • The phasing between the acoustic drivers has a negligible influence on the frequency where a pure standing wave is generated (resonance frequency). • When the porous material is exactly between the two acoustic drivers, the heat pumping happens in both directions, and the resulting temperature gradients are very small.
Yang et al. [57]	Traveling wave	Linear pressure wave generator	Stainless-steel cylinder filled with stainless-steel wire mesh with mesh number of 150	Connecting tubes made of stainless-steel and has diameter of 50 mm.	industrial waste heat recovery	Simulation using DelatEC	Copper shell-tube heat exchangers	Helium at 5 Mpa Frequency: 80 Hz	<ul style="list-style-type: none"> • The paper studied the usage of Travelling wave thermoacoustic heat pump for low temperature waste heat recovery. In other words, pumping heat from waste heat that has low temperature (40 – 70°C) to industrial processes that requires higher temperatures (120-150°C). • Increasing the regenerator length increases both the heating capacity and the consumed percentage of the total acoustic power. • At CHX and HHX temperatures of 70 and 150°C, respectively, the COP_h is 2.99, relative Carnot COP is 56.55%, and the heating capacity is 713.44 W.

References

- [1] G. W. Swift, *Thermoacoustics*. Cham: Springer International Publishing, 2017. Doi: [10.1007/978-3-319-66933-5](https://doi.org/10.1007/978-3-319-66933-5).
- [2] C. Sondhauss, "Ueber die Schallschwingungen der Luft in erhitzten Glasröhren und in gedeckten Pfeifen von ungleicher Weite," *Ann. Phys. Chem.*, vol. 155, no. 1, pp. 1–34, 1850, doi: [10.1002/andp.18501550102](https://doi.org/10.1002/andp.18501550102).
- [3] J. W. S. B. Rayleigh, *The Theory of Sound*. Macmillan, 1894.
- [4] N. Rott, "Damped and thermally driven acoustic oscillations in wide and narrow tubes," *Journal of Applied Mathematics and Physics (ZAMP)*, vol. 20, no. 2, pp. 230–243, Mar. 1969, doi: [10.1007/BF01595562](https://doi.org/10.1007/BF01595562).
- [5] N. Rott, "Thermoacoustics," *Advances in applied mechanics*, vol. 20, 1980.
- [6] J. Wheatley, T. Hofler, G. W. Swift, and A. Migliori, "An intrinsically irreversible thermoacoustic heat engine," *The Journal of the Acoustical Society of America*, vol. 74, no. 1, pp. 153–170, Jul. 1983, doi: [10.1121/1.389624](https://doi.org/10.1121/1.389624).
- [7] Hofler, T. J., "Thermoacoustic Refrigerator Design and Performance", PhDT, 1986.
- [8] T. J. Hofler, J. C. Wheatley, G. W. Swift, and A. Migliori, "Acoustic cooling engine," place = United States, year = 1988, month = 2.
- [9] S. Backhaus and G. W. Swift, "A thermoacoustic-Stirling heat engine: Detailed study," *The Journal of the Acoustical Society of America*, vol. 107, no. 6, pp. 3148–3166, Jun. 2000, doi: [10.1121/1.429343](https://doi.org/10.1121/1.429343).
- [10] G. W. Swift, "Thermoacoustic engines," p. 36.
- [11] M. E. Poese, R. W. M. Smith, S. L. Garrett, R. van Gerwen, and P. Gosselin, "Thermoacoustic refrigeration for ice cream sales," p. 8.
- [12] R. Smith, "Ben & Jerry's Uses Sound to Chill Ice Cream," *NPR*, Apr. 28, 2004. Accessed: Sep. 19, 2022. [Online]. Available: <https://www.npr.org/2004/04/28/1861434/ben-jerrys-uses-sound-to-chill-ice-cream>
- [13] "New roof top installation of SoundEnergy's thermoacoustic cooling system – SoundEnergy." <https://www.soundenergy.nl/new-roof-top-installation-of-soundenergys-thermoacoustic-cooling-system/> (accessed Sep. 19, 2022).
- [14] M. E. H. Tijani, "Loudspeaker-driven 15 nc our-acoustic refrigeration," 2001.
- [15] U. Ali, Y. Al Masalmeh, S. Abedrabbo, M. Islam, and I. Janajreh, "Numerical Simulation and Experimental Validation of Thermoacoustic Engine," in *ASME 2022 16th International Conference on Energy Sustainability*, Philadelphia, Pennsylvania, USA, Jul. 2022, p. V001T10A007. doi: [10.1115/ES2022-85821](https://doi.org/10.1115/ES2022-85821).
- [16] U. Ali, I. Janajreh, M. Islam and S. Abedrabbo, "Numerical Simulation Of Thermoacoustic Refrigerator Coupled With Thermoacoustic Engine", 15th International Conference On Heat Transfer, Fluid Mechanics And Thermodynamics Proceedings (HEFAT 2021), Pg. 1666-1671.
- [17] H. Wang *et al.*, "A looped heat-driven thermoacoustic refrigeration system with direct-coupling configuration for room temperature cooling," *Science Bulletin*, vol. 64, no. 1, pp. 8–10, Jan. 2019, doi: [10.1016/j.scib.2018.12.007](https://doi.org/10.1016/j.scib.2018.12.007).
- [18] I. A. Ramadan, H. Bailliet, G. Poignand, and D. Gardner, "Design, manufacturing and testing of a compact thermoacoustic refrigerator," *Applied Thermal Engineering*, vol. 189, p. 116705, May 2021, doi: [10.1016/j.applthermaleng.2021.116705](https://doi.org/10.1016/j.applthermaleng.2021.116705).
- [19] X. Wang, J. Xu, Z. Wu, and E. Luo, "A thermoacoustic refrigerator with multiple-bypass expansion cooling configuration for natural gas liquefaction," *Applied Energy*, vol. 313, p. 118780, May 2022, doi: [10.1016/j.apenergy.2022.118780](https://doi.org/10.1016/j.apenergy.2022.118780).
- [20] J. J. Wollan, G. W. Swift, S. Backhaus, and D. L. Gardner, "DEVELOPMENT OF A THERMOACOUSTIC NATURAL GAS LIQUEFIER," p. 8.
- [21] X. Xiao, X. Gu, and X. Zhang, "Combination of thermoacoustic heat dissipation with oscillating convection: A novel cooling method," *International Journal of Heat and Mass Transfer*, vol. 160, p. 120177, Oct. 2020, doi: [10.1016/j.ijheatmasstransfer.2020.120177](https://doi.org/10.1016/j.ijheatmasstransfer.2020.120177).
- [22] G. Chen and J. Xu, "Development of a small-scale piezoelectric-driven thermoacoustic cooler," *Applied Thermal Engineering*, vol. 213, p. 118667, Aug. 2022, doi: [10.1016/j.applthermaleng.2022.118667](https://doi.org/10.1016/j.applthermaleng.2022.118667).
- [23] O. G. Symko, E. Abdel-Rahman, Y. S. Kwon, M. Emmi, and R. Behunin, "Design and development of high-frequency thermoacoustic engines for thermal management in microelectronics," *Microelectronics Journal*, vol. 35, no. 2, pp. 185–191, Feb. 2004, doi: [10.1016/j.mejo.2003.09.017](https://doi.org/10.1016/j.mejo.2003.09.017).
- [24] R.-L. Chen, Y.-C. Chen, C.-L. Chen, C. Tsai, and J. DeNatale, "Development of miniature thermoacoustic refrigerators," presented at the 40th AIAA Aerospace Sciences Meeting & Exhibit, Reno,NV,U.S.A., Jan. 2002. Doi: [10.2514/6.2002-206](https://doi.org/10.2514/6.2002-206).
- [25] P. In 'T PHMW (Peter), "Mathematical aspects of thermoacoustics," Technische Universiteit Eindhoven, 2009. Accessed: Jul. 08, 2022. [Online]. Available: [https://research.tue.nl/en/publications/mathematical-aspects-of-thermoacoustics/d7880227-1951-4745-a3fb-9d7e1212593b\).html](https://research.tue.nl/en/publications/mathematical-aspects-of-thermoacoustics/d7880227-1951-4745-a3fb-9d7e1212593b).html)
- [26] J. P. Clark, W. C. Ward, and G. W. Swift, "Design environment for low-amplitude thermoacoustic energy conversion (DeltaEC)," *J. Acoust. Soc. Am.*, vol. 122, no. 5, p. 3014, 2007, doi: [10.1121/1.2942768](https://doi.org/10.1121/1.2942768).
- [27] A. A. Atchley, T. J. Hofler, M. L. Muzzerall, M. D. Kite, and C. Ao, "Acoustically generated temperature gradients in short plates," p. 13.
- [28] S. H. Tasnim, "Porous Media Thermoacoustic Stacks: Measurements and Models."
- [29] D. Gedeon, "Stirling, Pulse-Tube and Low-T Cooler Model Classes," p. 454.
- [30] A. Di Meglio and N. Massarotti, "CFD Modeling of Thermoacoustic Energy Conversion: A Review," *Energies*, vol. 15, no. 10, p. 3806, May 2022, doi: [10.3390/en15103806](https://doi.org/10.3390/en15103806).
- [31] "Analysis of a Coaxial, Compact Thermoacoustic Heat-Pump," *Acta Acustica united with Acustica*, vol. 99, no. 6, pp. 898–904, Nov. 2013, doi: [10.3813/AAA.918669](https://doi.org/10.3813/AAA.918669).
- [32] P. Saechan and A. J. Jaworski, "Numerical studies of co-axial travelling-wave thermoacoustic cooler powered by standing-wave thermoacoustic engine," *Renewable Energy*, vol. 139, pp. 600–610, Aug. 2019, doi: [10.1016/j.renene.2019.02.059](https://doi.org/10.1016/j.renene.2019.02.059).

- [33] M. E. H. Tijani and S. Spoelstra, "Study of a coaxial thermoacoustic-Stirling cooler," *Cryogenics*, vol. 48, no. 1–2, pp. 77–82, Jan. 2008, doi: [10.1016/j.cryogenics.2008.01.001](https://doi.org/10.1016/j.cryogenics.2008.01.001).
- [34] X. Wang, Z. Wu, L. Zhang, J. Hu, and E. Luo, "Traveling-wave thermoacoustic refrigerator for room temperature application," *International Journal of Refrigeration*, vol. 120, pp. 90–96, Dec. 2020, doi: [10.1016/j.ijrefrig.2020.08.021](https://doi.org/10.1016/j.ijrefrig.2020.08.021).
- [35] E. M. Sharify and S. Hasegawa, "Traveling-wave thermoacoustic refrigerator driven by a multistage traveling-wave thermoacoustic engine," *Applied Thermal Engineering*, vol. 113, pp. 791–795, Feb. 2017, doi: [10.1016/j.applthermaleng.2016.11.021](https://doi.org/10.1016/j.applthermaleng.2016.11.021).
- [36] M. A. Alamir, "An artificial neural network model for predicting the performance of thermoacoustic refrigerators," *International Journal of Heat and Mass Transfer*, vol. 164, p. 120551, Jan. 2021, doi: [10.1016/j.ijheatmasstransfer.2020.120551](https://doi.org/10.1016/j.ijheatmasstransfer.2020.120551).
- [37] N. V. Shivakumara and B. Arya, "Experimental Performance Evaluation of Thermoacoustic Refrigerator made up of Poly-Vinyl-Chloride for different Parallel Plate Stacks using Air as a working medium," *Materials Today: Proceedings*, vol. 22, pp. 2160–2171, 2020, doi: [10.1016/j.matpr.2020.03.285](https://doi.org/10.1016/j.matpr.2020.03.285).
- [38] P. Saechan and I. Dhuchakallaya, "A Study of Standing-Wave Thermoacoustic Refrigerator," vol. 9, no. 12, p. 6, 2015.
- [39] N. A. Zolpakar, N. Mohd-Ghazali, R. Ahmad, and T. Maré, "Performance of a 3D-printed Stack in a Standing Wave Thermoacoustic Refrigerator," *Energy Procedia*, vol. 105, pp. 1382–1387, May 2017, doi: [10.1016/j.egypro.2017.03.513](https://doi.org/10.1016/j.egypro.2017.03.513).
- [40] J. Kajurek, A. Rusowicz, and A. Grzebielec, "The Influence of Stack Position and Acoustic Frequency on the Performance of Thermoacoustic Refrigerator with the Standing Wave," *Archives of Thermodynamics*, vol. 38, no. 4, pp. 89–107, Dec. 2017, doi: [10.1515/aoter-2017-0026](https://doi.org/10.1515/aoter-2017-0026).
- [41] L. D. Landau and E. M. Lifshitz, *Fluid Mechanics*, Second Edition: Volume 6 (Course of Theoretical Physics), 2nd ed. Butterworth-Heinemann, 1987.
- [42] A. I. Abd El-Rahman, W. A. Abdelfattah, K. S. Abdelwahed, A. Salama, A. Rabie, and A. Hamdy, "A compact standing-wave thermoacoustic refrigerator driven by a rotary drive mechanism," *Case Studies in Thermal Engineering*, vol. 21, p. 100708, Oct. 2020, doi: [10.1016/j.csite.2020.100708](https://doi.org/10.1016/j.csite.2020.100708).
- [43] A. A. Rahman and X. Zhang, "Single-objective optimization for stack unit of standing wave thermoacoustic refrigerator through fruit fly optimization algorithm," *International Journal of Refrigeration*, vol. 98, pp. 35–41, Feb. 2019, doi: [10.1016/j.ijrefrig.2018.09.031](https://doi.org/10.1016/j.ijrefrig.2018.09.031).
- [44] G. Chen, L. Tang, and Z. Yu, "Modeling and analysis of a dual-acoustic-driver thermoacoustic heat pump," *Thermal Science and Engineering Progress*, vol. 30, p. 101270, May 2022, doi: [10.1016/j.tsep.2022.101270](https://doi.org/10.1016/j.tsep.2022.101270).
- [45] H. Wang et al., "Study on a novel looped heat-driven thermoacoustic refrigerator with direct-coupling configuration for room temperature cooling," *International Journal of Refrigeration*, vol. 123, pp. 180–188, Mar. 2021, doi: [10.1016/j.ijrefrig.2020.11.019](https://doi.org/10.1016/j.ijrefrig.2020.11.019).
- [46] J. Chi, J. Xu, L. Zhang, Z. Wu, J. Hu, and E. Luo, "Study of a gas-liquid-coupled heat-driven room-temperature thermoacoustic refrigerator with different working gases," *Energy Conversion and Management*, vol. 246, p. 114657, Oct. 2021, doi: [10.1016/j.enconman.2021.114657](https://doi.org/10.1016/j.enconman.2021.114657).
- [47] A. Widyaparaga, T. Hiromatsu, T. Koshimizu, D. Deendarlianto, M. Kohno, and Y. Takata, "Thermoacoustic heat pumping direction alteration by variation of magnitude and phase difference of opposing acoustic waves," *Applied Thermal Engineering*, vol. 101, pp. 330–336, May 2016, doi: [10.1016/j.applthermaleng.2016.02.032](https://doi.org/10.1016/j.applthermaleng.2016.02.032).
- [48] R. Rahpeima and R. Ebrahimi, "Numerical investigation of the effect of stack geometrical parameters and thermo-physical properties on performance of a standing wave thermoacoustic refrigerator," *Applied Thermal Engineering*, vol. 149, pp. 1203–1214, Feb. 2019, doi: [10.1016/j.applthermaleng.2018.12.093](https://doi.org/10.1016/j.applthermaleng.2018.12.093).
- [49] M. A. Elaziz, A. H. Elsheikh, and S. W. Sharshir, "Improved prediction of oscillatory heat transfer coefficient for a thermoacoustic heat exchanger using modified adaptive neuro-fuzzy inference system," *International Journal of Refrigeration*, vol. 102, pp. 47–54, Jun. 2019, doi: [10.1016/j.ijrefrig.2019.03.009](https://doi.org/10.1016/j.ijrefrig.2019.03.009).
- [50] İ. Gökay and R. Karabacak, "Experimental investigation of the effect of different waveforms on heat transfer in a thermoacoustic cooler," *International Journal of Refrigeration*, vol. 129, pp. 259–266, Sep. 2021, doi: [10.1016/j.ijrefrig.2021.04.015](https://doi.org/10.1016/j.ijrefrig.2021.04.015).
- [51] A. Widyaparaga, T. Hiromatsu, Deendarlianto, M. Kohno, and Y. Takata, "Acoustic field alteration in a 100 Hz dual acoustic driver straight tube travelling wave thermoacoustic heat pump for thermoacoustic heat transport control," *International Journal of Heat and Mass Transfer*, vol. 151, p. 119274, Apr. 2020, doi: [10.1016/j.ijheatmasstransfer.2019.119274](https://doi.org/10.1016/j.ijheatmasstransfer.2019.119274).
- [52] J. Xu, J. Hu, E. Luo, J. Hu, L. Zhang, and S. Hochgreb, "Numerical study on a heat-driven piston-coupled multi-stage thermoacoustic-Stirling cooler," *Applied Energy*, vol. 305, p. 117904, Jan. 2022, doi: [10.1016/j.apenergy.2021.117904](https://doi.org/10.1016/j.apenergy.2021.117904).
- [53] G. Harikumar, K. H. Ho, K. Wang, S. Dubey, and F. Duan, "Thermoacoustic energy conversion in a square duct," *Energy Procedia*, vol. 158, pp. 1811–1816, Feb. 2019, doi: [10.1016/j.egypro.2019.01.425](https://doi.org/10.1016/j.egypro.2019.01.425).
- [54] H. Wang et al., "A novel looped low-temperature heat-driven thermoacoustic refrigerator operating in room temperature range," *Energy Procedia*, vol. 158, pp. 1653–1659, Feb. 2019, doi: [10.1016/j.egypro.2019.01.386](https://doi.org/10.1016/j.egypro.2019.01.386).
- [55] S. Gh. Yahya, X. Mao, and A. J. Jaworski, "Experimental investigation of thermal performance of random stack materials for use in standing wave thermoacoustic refrigerators," *International Journal of Refrigeration*, vol. 75, pp. 52–63, Mar. 2017, doi: [10.1016/j.ijrefrig.2017.01.013](https://doi.org/10.1016/j.ijrefrig.2017.01.013).
- [56] G. Chen and J. Xu, "Active control of heat transport inside the porous material of a looped-tube dual-acoustic-driver thermoacoustic refrigerator," *Cryogenics*, vol. 125, p. 103516, Jul. 2022, doi: [10.1016/j.cryogenics.2022.103516](https://doi.org/10.1016/j.cryogenics.2022.103516).
- [57] Z. Yang, Y. Zhuo, L. Ercang, and Z. Yuan, "Travelling-wave thermoacoustic high-temperature heat pump for industrial waste heat recovery," *Energy*, vol. 77, pp. 397–402, Dec. 2014, doi: [10.1016/j.energy.2014.09.023](https://doi.org/10.1016/j.energy.2014.09.023).